Inverse heat conduction problem: estimation of a source term for an electron beam welding; theoretical and experimental validations

Philippe Le Masson, Sébastien Rouquette, Tahar Loulou, Eugène Artioukhine

III European Conference on Computational Mechanics
Solids, Structures and Coupled Problems in Engineering
C.A. Mota Soares et.al. (eds.)
Lisbon, Portugal, 5–8 June 2006

INVERSE HEAT CONDUCTION PROBLEM: ESTIMATION OF A SOURCE TERM FOR AN ELECTRON BEAM WELDING; THEORETICAL AND EXPERIMENTAL VALIDATIONS.

P. Le Masson [1], S. Rouquette [2], T. Loulou[1] and E. Artioukhine[3]

[1] Laboratoire d'Etudes Thermique Energétique et Environnement. Université de Bretagne Sud, Centre de recherche, rue de saint Maudé, F-56321 Lorient Cedex.
philippe.le-masson @univ-ubs.fr
tahar.loulou@univ-ubs.fr

[2] Laboratoire des Systèmes Mécaniques et Ingénierie Simultanée (LASMIS) FRE CNRS 2719. Université de Technologie de Troyes, F-10010 TROYES Cedex.
sebastien.rouquette@utt.fr

[3] Institut FEMTO-ST, Département CREST, CNRS UMR 6174, 2 avenue Jean Moulin, 90000 Belfort, France.
eugene.artioukhine@univ-fcomte.fr

Keywords: Inverse problems, welding, heat transfer, source term.

Abstract. *This paper is concerned with the estimation of a heat source applied in the electron beam welding process by using temperature measurements in solid phase. The aim is to identify the energy distribution which is applied in the liquid and vapor zones. This identification is realized at each time in a longitudinal plane or in a transversal plane perpendicularly to the welding axis. For this work, the goals are the estimation of the energy distribution in a real case. The thermometallurgical model does not take into account the convective phenomena in the fused zone. We show the development of the experimentation, its realization and the exploitation of measurements. At last, the Levenberg Marquardt, the Iterative Regularization Method and the measurements will be used for this two-dimensional metallurgical inverse heat transfer problem.*

1 INTRODUCTION

Welding is a complex process that involves many influent parameters on the final solidification structure and the properties of the welded joint. The first stage is to choose these parameters which lead to an acceptable welding quality. The main difficulty of the theoretical analysis is that the exact distribution of the thermal energy absorbed and generated in the liquid and vapor zones is not easy to predict and cannot be measured directly. When studying the welding, the theoretical analysis uses complementary experimental information: the temperature measurements near the liquid zone (in the heat affected zone) and the microstructural properties (optical micrograph...). The objective of this work is the estimation of the energy distribution in the welding zone. It is difficult to estimate correctly the energy distribution from the temperature measurements taken at points which are too far from the welding zone. In fact, the temperature difference between the welding and solid zones is big enough. There is a strong damping effect in the solid zone. Many works deal with the estimation of boundary conditions or the determination of distributed heat flux on the boundary of the body [1-3]. Few of these works consider experimental situations involving unknown heat sources. Silva Neto and Ozisik [4] used the conjugate gradient algorithm to estimate the time-varying strength of a line source placed in a rectangular region with insulated boundaries, but the location of the source was specified. Le Niliot [5] studied linear inverse problems with two point heat sources, and experimental results were presented in [6].

In many studies, the inverse fusion and solidification problem has been analysed using a simplified approach based on only a conduction model in the liquid and vapor zones. Under these assumptions, 1D or 2D Stefan problems taking into account only the conduction effects in all the phases during the process were considered. The objective was to estimate an energy distribution [3], or a motion of the solid-liquid interface [7-10]. Another approach was to take into account the convection effects describing the Navier-Stokes equations in the liquid and vapor zones [11]. Mixed approaches were employed, in which an apparent source term is determined in the liquid and vapor zones representing the different phenomena [12]. At last, we can find applications which use the inverse technique and Bézier splines for identifying the location of the liquid solid interface by solving an inverse geometry problem [13].

In this paper, we use the first hypothesis for the electron beam welding process. We consider only the conduction effects for all phases (solid, liquid and vapor). The Levenberg Marquardt [14] and the iterative regularization method [2] are used to estimate the dissipation energy in the liquid and vapor zones. First, we present the electron beam welding technique and the used steel sample. Second, we describe the direct problems including the simulation of phase transformations and the source term (electron beam). Third, the estimation procedures are described. Finally, the experimentation and the estimation results are discussed.

2 THE ELECTRON BEAM WELDING

2.1 Principle

The electron beam (EB) welding is an assembling process in vacuum using a high density energy beam. This technique permits the welding of the high thicknesses (up to 16 cm) with a low width and a narrow Heat Affected Zone (HAZ). At the beginning of the welding process, the high power density of the EB leads to an evaporation of the material and then to a keyhole (Figure 1). It is this keyhole and its displacement which generate the welded joint. The high penetration capacity of the beam with a narrow fusion zone characterizes the EB welding in comparison with other weld methods. For these other methods, the penetration is limited by the heat conduction [15].

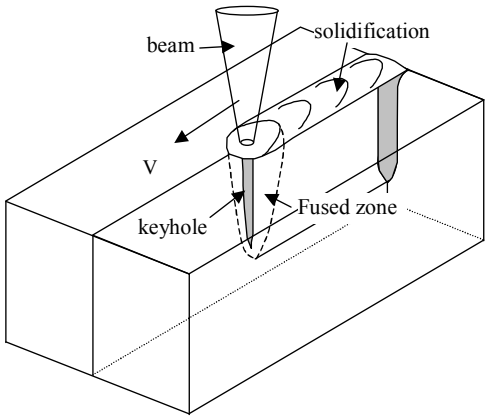

Figure 1. Welding process.

For this study, weld joints are used which are realized in the "Direction des Constructions Navales" (DCN) in Indret (44-France) (power of this EB: 100KW). The welds are made of 18MnNiMo 5 steel samples (ASTM A508 Cl.3). In this paper, a partial penetration welded joint is analyzed. Figure 2 shows the micrography of this sample which is used to determine precisely the locations of the measurement points by using a scan of this welding joint. The high temperature level in the fusion and vapor zones prevents the installation of the thermocouples in these zones. The used thermocouples are thus located in the Heat Affected Zone (HAZ) (750°C< T< 1450°C).The welding parameters are: voltage: U=60kV, current I = 0.29A, velocity V = 2.5mm/s, focus current I_f=2.46A.

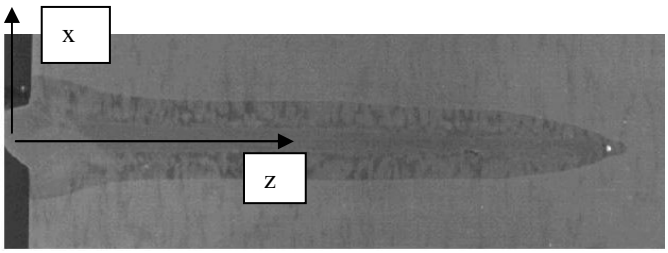

Figure 2. Weld joint.

With the experimental temperatures obtained from the thermocouples and corresponding diagrams (CCT or TTT) we will validate the simulation of the metallurgical transformations by comparing the experimental and simulated thermal and metallurgical parameters. Furthermore, temperatures computed at the thermocouple locations by solving the direct problem will be used to estimate the source term in the fusion and vapor zones.

2.2 Numerical simulation of the electron beam welding

Several works are concerned with the numerical simulation of the EB welding in the laboratory LET2E [16, 17, 18]. In these works, the SYSWELD code [19] was used. Normally, this problem is a 3D problem and the equations are the heat conduction equation (1) and the metallurgical kinetic equations (2) of the type Leblond and Devaux [20] and Koistinen and Marburger [21]:

$$\rho(T)C_p(T)\frac{\partial T}{\partial t}=\frac{\partial}{\partial x}\left(\lambda(T)\frac{\partial T}{\partial x}\right)+\frac{\partial}{\partial y}\left(\lambda(T)\frac{\partial T}{\partial y}\right)+\frac{\partial}{\partial z}\left(\lambda(T)\frac{\partial T}{\partial z}\right)+\frac{\partial P_\alpha}{\partial t}L_{\alpha\gamma}(T) - \frac{\partial(\rho H)}{\partial t}+S(x,y,z,t) \quad (1)$$

$$\frac{\partial P}{\partial t}=\frac{P_{eq}-P}{\tau}f\left(\frac{\partial T}{\partial t}\right) \text{ and } P=P_{\max}\left(1-\exp\left(-b\left(T-M_s\right)\right)\right) \quad (2)$$

The boundary and initial conditions are the following: at the lower, upper and lateral surfaces, only the radiative conditions are fixed because the welding process is carried out in vacuum. For example, at the lower surface, the boundary condition is:

$$-\lambda(T)\frac{\partial T(x,y,z=0,t)}{\partial z}=\varepsilon\sigma\left[T^4(x,y,z=0,t)-T_{\inf}{}^4\right] \quad (3)$$

On the axis:

$$\frac{\partial T(x=0,y,z,t)}{\partial x}=0 \quad (4)$$

Initial conditions: $T(x, y, z, 0) = T_0$; $P_\alpha(x, y, z, 0) = 1$ (5)

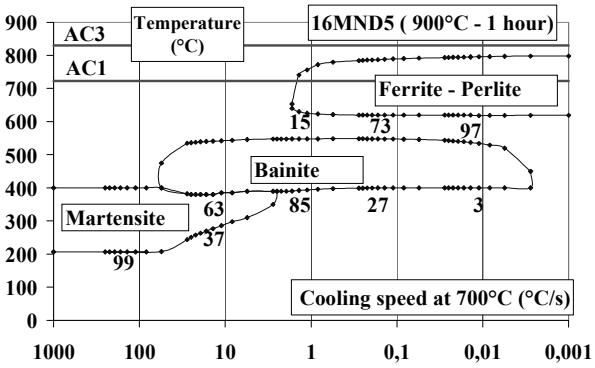

Figure 3. CCT diagram.

In the heat conduction equation (1), the source terms $\frac{\partial P_\alpha}{\partial t}L_{\alpha\gamma}(T)$ and $\frac{\partial(\rho H)}{\partial t}$ allow to take into account the phase change enthalpy according to the temperature of the sample (metallurgical transformations for the first term - P_α is the proportion of metallurgic phase α, fusion and evaporation for the second). The transformation energy is calculated according to the phase enthalpy: $L_{\alpha\gamma}(T)=\rho_\gamma H_\gamma-\rho_\alpha H_\alpha$ and by considering two metallurgical phases only: γ (austenite) and α (ferrite, perlite, bainite or martensite). The enthalpies of the phases α and γ are computed with the use of polynomial functions between 100 °C and 1450 °C. The parameters of the metallurgical kinetic equations are calculated by simulating the CCT diagram (Figure 3).

For each time and space node, the cooling speed and the temperature value are used. With this information, the percentage P_i of the metallurgical transformation is computed. Moreover, the thermophysical characteristics $\rho(T), C(T)$ and $\lambda(T)$ are calculated at all time steps by a law of mixtures according to the temperature, e.g. $\lambda(T)=P_\gamma * \lambda_\gamma(T) + P_\alpha * \lambda_\alpha(T) = \sum_i P_i \lambda_i(T)$.

For the phase γ and for T < 1450°C:

$\rho_\gamma * C_\gamma(T)$ =3641440+4638.78*T-11.7784 *T^2 +0.0155136*T^3-9.29165E-6*T^4+2.03093E-9*T^5
$\lambda_\gamma(T)$ =0.0148939+1.24115E-5*T-7.74533E-10*T^2 +8.11438E-13*T^3
For the phase α and for T < 750°C:
$\rho_\alpha * C_\alpha(T)$ =3620850+2955.1*T-7.52398*T^2 +0.0249182*T^3-1.68686E-5*T^4
$\lambda_\alpha(T)$ =0.0525037-3.35115E-5*T+1.76665E-8*T^2 -1.74307E-11*T^3
The other thermal transformations are computed between 1450°C and 1550°C for the fusion and between 2600°C and 2800°C for the evaporation. These enthalpies are given in Costantini work [15]: $\Delta H_{fus} = 391970\, J/kg$ and $\Delta H_{vap} = 6332879\, J/kg$. At last, the thermophysical characteristics of the liquid and vapor phases are computed at the temperature 1450°C.

The initial data of the model is:
-The mesh;
-The thermophysical characteristics $\rho(T), C(T)$, $\lambda(T)$ and $L_{\alpha\gamma}$ for the different phases according to the temperature;
-The initial and final temperatures of thermal transformations for all phases (CCT diagram);
-The initial temperature T_0 = 20 °C in whole domain;
-The ambient temperature T_{inf} ;
-The emissivity of the considered material is supposed to be constant and equal to 0.8.
-The theoretical source is a Gaussian source:

$$S(x,y,z,t) = f(z) * \frac{8\eta U I_b}{\pi \Phi_E^2} \exp\left(-\frac{8\left(x^2+(y-Vt)^2\right)}{\Phi_E^2}\right) \text{ with } f(z) = \frac{2}{h}\left(1-\frac{z}{h}\right) \quad (6)$$

This 3D problem is very time consuming in computation. Also, we use 2D models preferably. In this study, we use two numerical simulations: the first in the longitudinal plane and the second in the transversal plane (figure 4)

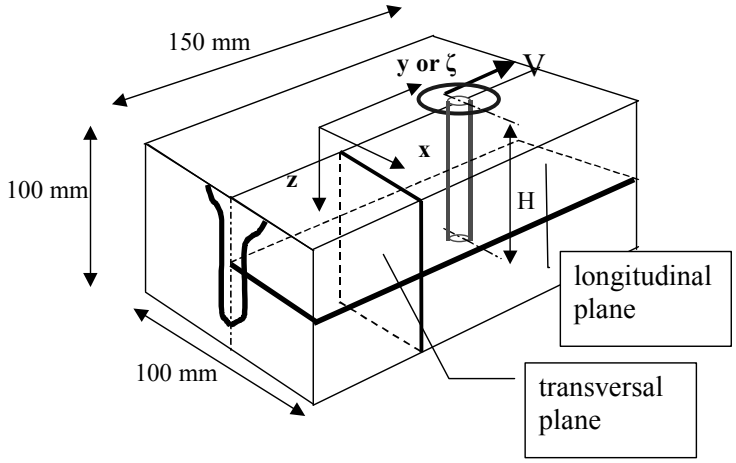

Figure 4: The studied planes

2.2.1. Numerical simulation in the longitudinal plane

In this first simulation, the studied domain is one half of the longitudinal section taken perpendicularly to the beam axis (Figure 4). For this study, we use a quasi stationary problem and we define moving coordinate system (x, y), where $y=\xi+Vt$. In the stationary regime

($\frac{\partial T}{\partial t}=0$), the heat conduction equation and the metallurgical kinetic equations become (7) and (8):

$$VC(T)\frac{\partial T}{\partial y}=\frac{\partial}{\partial x}\left(\lambda(T)\frac{\partial T}{\partial x}\right)+\frac{\partial}{\partial y}\left(\lambda(T)\frac{\partial T}{\partial y}\right)+V\frac{dP_\alpha}{dy}L_{\alpha\gamma}(T)-V\frac{\partial(\rho H)}{\partial y}+S(x,y) \quad (7)$$

$$V\frac{dP}{dy}=\frac{P_{eq}-P}{\tau}f\left(\frac{dT}{dy}\right) \text{ and } P=P_{\max}\left(1-\exp\left(-b(T-M_s)\right)\right) \quad (8)$$

For this new problem, we take only a part of the longitudinal section. The boundary conditions in the beam direction " y " change and we set these new conditions:

$$\text{at } y=y_{\min} \ \mathbf{T=T_0} \quad \text{and} \quad \text{at } y=y_{\max} \ \frac{\partial T}{\partial y}=0 \quad (9)$$

For the conditions in the transverse direction " x ", we have the same boundary conditions. Figure 5 shows the study section with the new conditions.

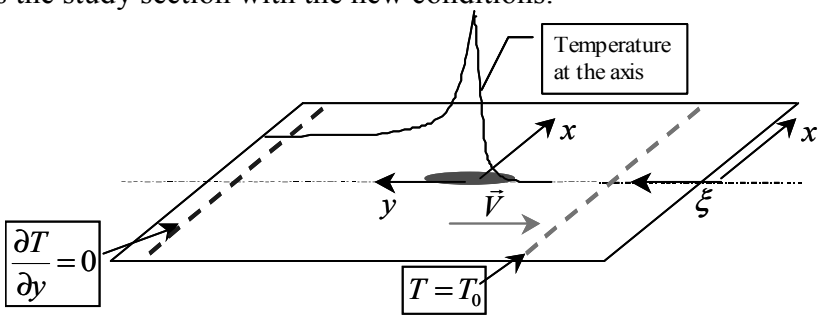

Figure 5 : Studied section

In the equation (7), the term $S(x,y)$ is the source term which represents the energy of the electron beam.

$$S(x,y)=f(z_e)*\frac{8\eta UI_b}{\pi\Phi_E^2}\exp\left(\frac{8\left(x^2+(y-y_S)^2\right)}{\Phi_E^2}\right) \text{ with } f(z_e)=\frac{2}{h}\left(1-\frac{z_e}{h}\right) \quad (10)$$

where the parameters are : efficiency coefficient $\eta=0.9$, voltage: $U=60\,kV$, current: $I_b=0.29A$, velocity: $V=2.5\,mm.s^{-1}$, penetration: $h=71\,mm$, beam diameter: $\phi_E=1\,mm$ and z_e: the depth of the longitudinal section.

The goal with this simulation is the estimation of the parameters describing the source term by the well known Levenberg-Marquardt method [14]. So, first, the source term which has been presented above is defined mainly by three parameters (P_W, W_{FE}, y_S):

$$S(x,y)=\frac{P_W}{W_{FE}^2}\exp\left(-\left(\frac{x^2+(y-y_S)^2}{W_{FE}^2}\right)\right) \quad (11)$$

Where P_W is the power of the electron beam, W_{FE}, equal to $\sqrt{\phi_E^2/8}$, is the parameter of the Gaussian source and y_S is the position of the source in this quasi steady problem.

We analyse only a linear problem without metallurgical transformations and with constants thermophysical characteristics: $\rho=7500$ kg.m^{-3}, $Cp=520$ J.kg^{-1}.K^{-1}, $\lambda=32$ W.K^{-1}.m^{-1} and $\varepsilon=0.8$. The parameters values of the Gaussian source are estimated as follows : $P_W=\frac{2}{h}\left(1-\frac{z_e}{h}\right)\left(\frac{\eta UI}{\pi}\right)$

with $z_e = 0.041\,m$, $h = 0.071\,m$, $\eta = 0.9$, $U = 60\,kV$ and $I_b = 0.29\,A$ lead to $P_W \approx 60\,kW.m^{-1}$; $y_S = 0.015\,m$; $W_{FE} = \sqrt{\phi_E^2/8}$ with $\phi_E = 1\,mm$ the experimental beam diameter gives $W_{FE} = 3.53\,10^{-4}\,m$. These results are computed using Femlab 2.3 finite element code [16].

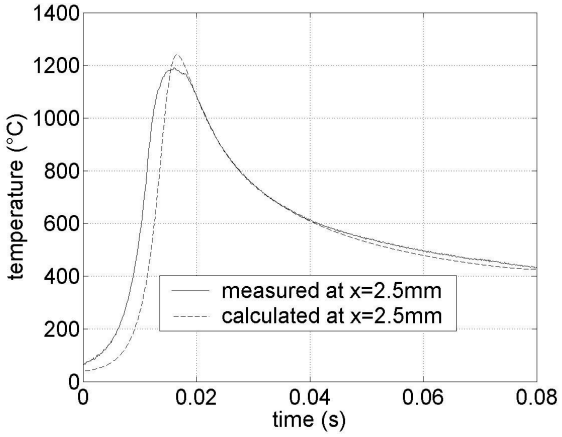

Figure 6. Comparison between the experimental and computed temperatures.

The Figure 6 shows the comparison between the experimental data and numerical results. Globally, we find a good level for the maximal temperatures. There are still problems because we do not take into account the effects in the axial of the beam and we have an adiabatic condition in $y = y_{max}$.

2.2.2. Numerical simulation in the transversal plane

Here, we use a code analogous to SYSWELD which is incorporated in the developed estimation code. The finite difference method based on an implicit scheme is used to solve the direct and inverse problems. The studied domain is one half of the transversal plane taken perpendicularly to the welding axis (Figure 4). So, in the equations (1) to (6), the coordinate y disappears.

The set of equations is solved with the use of a fine discretization of the domain near the EB zone (176 nodes in the vertical direction; 52 nodes in the transverse direction). The finite difference grid is uniform in the vertical direction, $\Delta z = 0.5$ mm, and not uniform in the transverse direction, $0.05\text{mm} < \Delta x < 2$ mm. The direct problem and the corresponding code have been verified in previous papers [16, 17, 18].

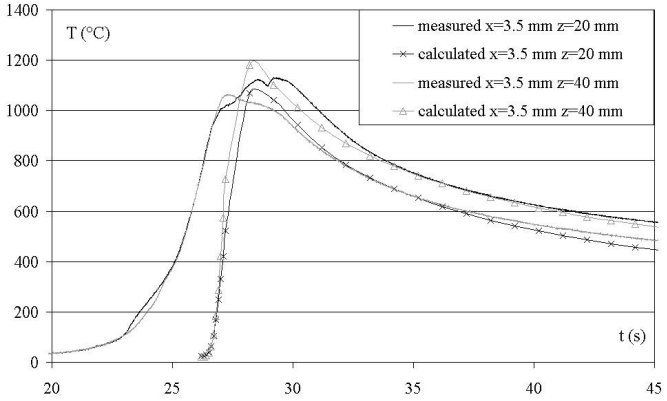

Figure 7. Comparison between the experimental and numerical temperatures.

The figure 7 shows the comparison between the experimental data and numerical results for a Gaussian source [16]. Globally, we find a good level for the maximal temperatures. Some problems stay because we do not have the diffusion effect forward the beam.

For the reasons seen in two simulations, it seems to be important to estimate an apparent source term for modelling the diffusion effect in the steel.

3 THE INVERSE PROCEDURES

The objective of this research is to determine a source term. The determination is conducted from the temperature values measured in the heat affected zone at a distance between 2 mm and 8 mm from the welding axis.

3.1 The Estimation with the Levenberg Marquardt [14]

The inverse problem consists in the minimization of a quadratic functional $J(P)$ where $P=\{P_W, W_{FE}, y_S\}$ is the set of unknown parameters. The solution of the inverse problem is obtained when the minimization of the difference between the calculated and measured temperatures is realized.

$$J(P)=\left[Y_i-T_i\right]^T\left[Y_i-T_i\right] \tag{12}$$

where Y_i are the measured temperatures and T_i the calculated temperatures. This method is useful when the number of the parameters to identify is low. This technique is an iterative method for solving non linear least squares problems of the parameter estimation [14]. In the thesis of Jialin Guo [16], we can find all the theoretical developments of the method. Here, we will simply point out the principal conclusions of this analysis:

- First, the analysis of the normalised sensitivity coefficients of the three parameters shows that the coefficients W_{FE} and y_S are linearly dependent along the longitudinal axis. Due to this behavior for these two parameters, simultaneous identification of these two parameters by Levenberg-Marquardt is not possible. In conclusion, the identifications seem to be possible in the domain around the source position for the couples (P_W, y_S) and (P_W, W_{FE}).
- Second, the low magnitude of the sensitivity coefficient W_{FE} leads to a difficulty in the estimate of this parameter W_{FE}, the "diameter of the beam welding". In the same way, we will show that it is difficult to obtain the lateral distribution of energy.

3.2 The Estimation with the Iterative Regularization Method

The use of the iterative regularization method [2] leads to the variational formulation of the inverse problem of estimating the source term and the residual functional minimization by utilizing the unconstrained conjugate gradient method. The residual functional is defined as:

$$J(S)=\frac{1}{2}\int_0^{t_f}\sum_{j=1}^{N}\left[T\left(x_j,z_j,t;S\right)-Y_j\left(t\right)\right]^2 dt \tag{13}$$

where $T\left(x_j,z_j,t;S\right)$ and $Y_j\left(t\right)$ are the computed and measured temperature histories, respectively, at N various measurement points of the material. The inverse algorithm consists in minimizing this residual functional under constraints on the temperature given by the direct problem (equations (1) to (5)). The steps of this procedure are described in the thesis of Jialin Guo [16]. We can note that three systems of equations (direct, in variation and adjoint) are solved numerically using a finite difference method and an implicit scheme. The time step used in the estimation is Δt=0.01s and the discretization on the welding axis is Δz=0.5mm and Δx=0.05mm.

Here again, we will simply point out the principal conclusions of this analysis:

- On the welding axis the maximum calculated temperature is around 6000°C and the maximum temperature in the heat affected zone is around 1400°C. This demonstrates the high damping in the material. The calculus of the Fourier number shows the difficulty of the estimation. It is calculated with average values: $a=5\ 10^{-6}$ m²/s, $\Delta x=1.5$mm, $\Delta t=0.001$s and it is equal to $\Delta Fo=0.002$. In fact, generally, we have no problem for the source estimation when the Fourier number is greater than 0.1.
- The analysis of the estimation results permits to underscore the following points: If we compare the exact and estimated temperatures, it can be seen that the results are good enough. But after 200 iterations, we do not correctly find the Gaussian shape of the source term in transversal direction (Figures 8 and 9). Globally, we find the average values of the source. On the other hand, the Gaussian form, as a function of time, is correct. An analysis of this mean heat distribution depending on the depth shows that the estimated form follows well the exact function $f(z,h) = \frac{2}{h}\left(1-\frac{z}{h}\right)$. Finally, one can see that it is more difficult to obtain the convergence to the exact source term for the beginning of the welding process. This difficulty comes from the fact that there is no conduction effect forward the beam (only a transversal plan is analyzed). So, the temperature variation is very abrupt when the beam arrives at the study plan. In reality, the thermocouples give information on the beam due to the conduction effects and it is easier to estimate the source term at the beginning of the welding process.

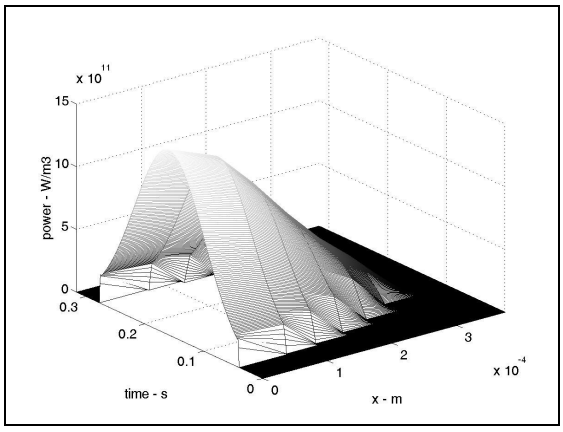

Figure 8. Exact Gaussian source at z=0.

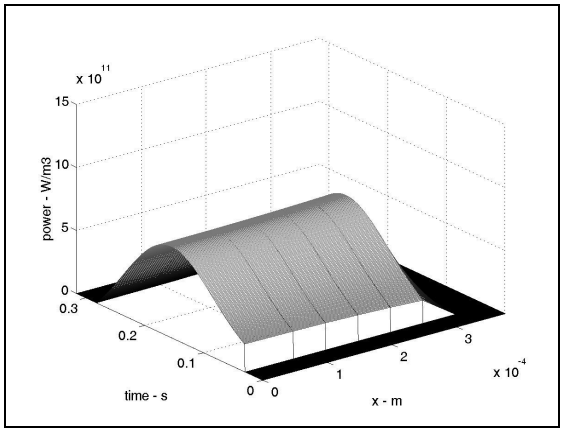

Figure 9. Estimated source at z=0.

4 THE EXPERIMENTAL SETUP

The numerical estimation of the source term (test cases) by different methods [16] has shown that it is difficult to obtain the space distribution of energy in each plane perpendicular to the welding axis. On the other hand, the distribution of energy according to the depth as well as the relative position of the source with respect to this depth remains potentially identifiable. The presented experimental work was carried out in the laboratory LET2E since 2000 [22]. This lead us to propose a method of thermocouple installation based on the cutting of the samples in order to carry out a fine instrumentation inside the samples [16, 22]. Figure 10 presents the principle of cutting of the samples.

First of all, with the temperature level reached in the molten zone and with the choice of the type of thermocouple (type K – 50µm), we have localized the isotherm 1300°C on the macrography (figure 2) by using the direct model. The thermocouples were thus positioned

around this isotherm 1300°C +/- 0.3mm. The figure 11 presents the selected thermocouples positions. On this figure, it appears four colors corresponding to four interfaces. For practical reasons, we have carried out two samples of 3 blocks having 2 interfaces equipped with thermocouples. The red interface (R :n°4) (23 thermocouples) and the blue interface (B :n°1) (24 thermocouples) on the first sample (figure 12) and the black interface (N :n°3) (23 thermocouples) and the green interface (V :n°2) (23 thermocouples) on the second sample

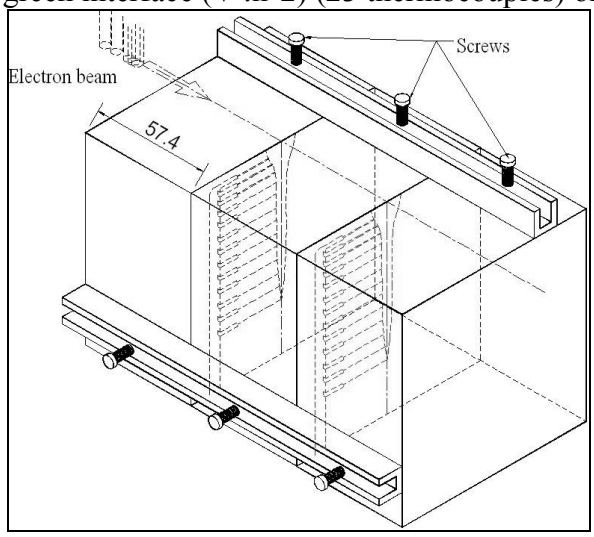

Figure 10. First block.

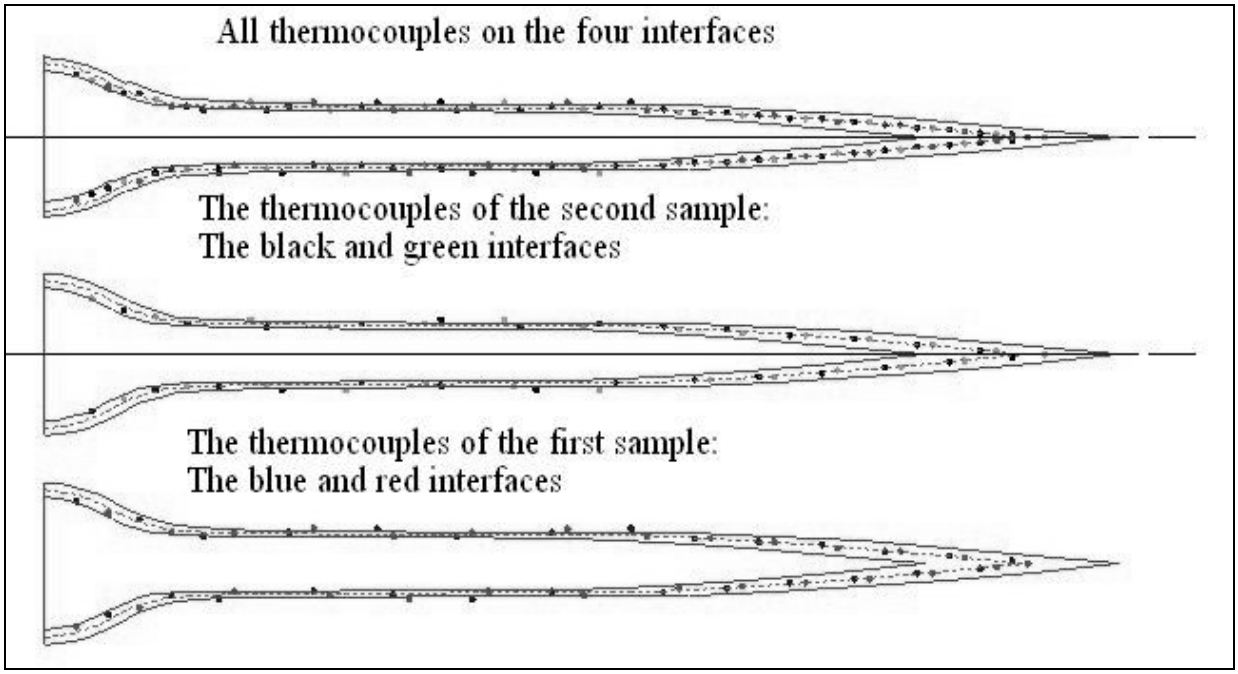

Figure 11: The four interfaces

The figure 12 shows the principle of the instrumentation. The sensors were located mainly in the heat affected zones. Each thermocouple is welded by capacitive discharge at the bottom of a small hole (diameter 400 µm, depth 500 µm). The wires of 50 µm diameter are then brought out on figure 12, we see the grooves obtained by electroerosion to a basin (with approximately 20mm of the axis of welding) where a connection with wires of 125 µm is carried

out. The wires are then protected and insulated electrically by a high temperature adhesive (Aremco Ceramabond 571 - Tmax = 1750°C) and by an elastomer (T < 470°C). After the thermocouple installation, the blocks are welded at some points.

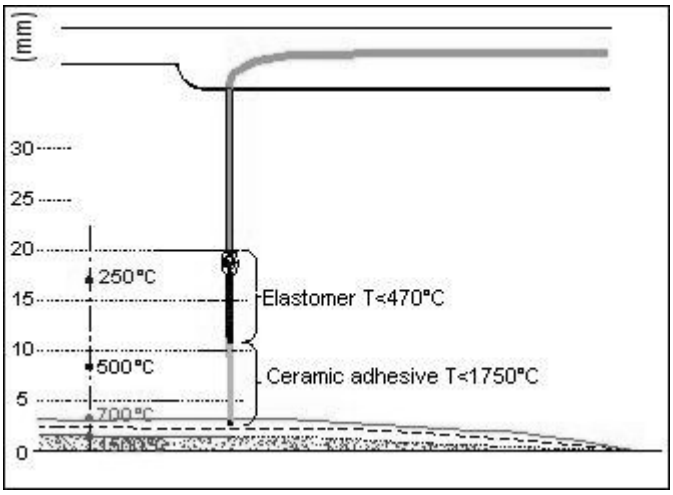

Figure 12. Thermocouple installation.

The EB welding experiment was developed on the industrial site of the DCN establishment. The EB welding machine has a power of 100 KW with a vacuum chamber volume of 800 m^3. A "ARATA" type test [23] was carried out on a strip iron stainless to ensure the reproducibility of the beam form with the shooting reference parameters of welding (U = 60 kV, I_b = 0,29 A, I_f = 2.46 A, V = 2.5 mm /s, distance of shooting = 160 mm). Indeed, the geometry of the beam can change according to the installation ageing. Lastly, the frequency of acquisition is chosen to be 100 Hz over a total recording time of 5 minutes. With the two samples, we have collected 93 thermal cycles, 52 thermocouples gave very clean recordings which can be used directly in the estimation code, 28 thermocouples gave truncated information and 13 thermocouples exceeded the acceptable temperature range given by a K type sensor. The figure 13 shows an example of truncated recording.

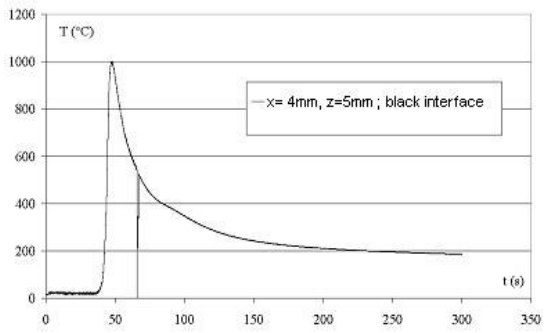

Figure 13: a truncated recording

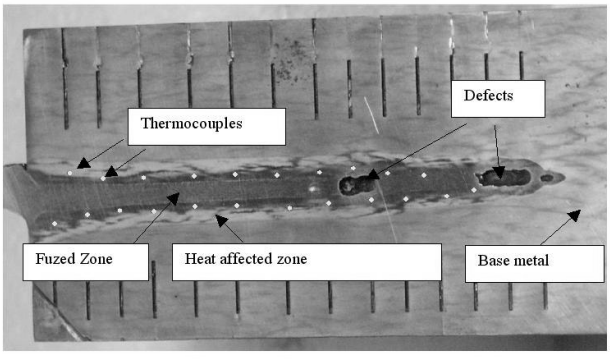

Figure 14: the rectified interface

The last stage of this experimental work consists in an accurate check of the thermocouple locations which is essential to estimate accurately the source term and in a synchronization of the measurements taken on the four interfaces [16]. For this reason, we cut out then rectified the samples to appear the thermocouples (figure 14).

In order to define the exact position of the points of measurements, we worked under binocular provided with a camera and a computer on which software enabled us to make statements of dimensions (figure 15):

$$x_{real} = \frac{a+b}{2} \quad (+/-0.2\,mm) \tag{14}$$

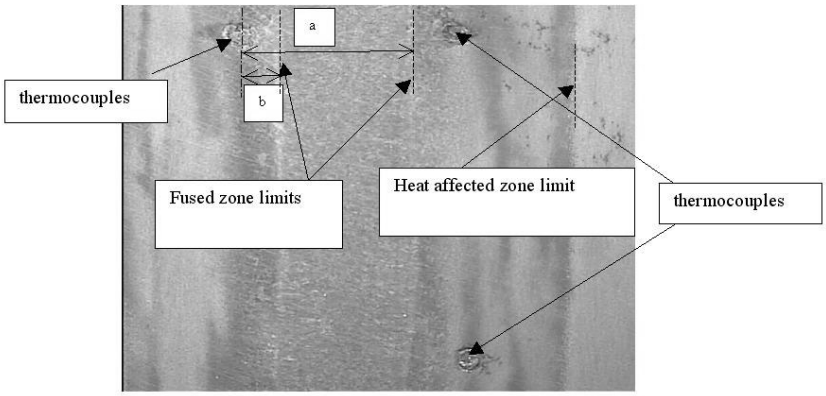

Figure 15: measure positions of the thermocouples

5 THE ESTIMATION

The estimation of the source term is based on 52 temperature profiles obtained on the four interfaces after a temporal retiming.

5.1 Estimation of the parameters with the Levenberg Marquardt

Measure R26	x (m)	z (m)	P_W (W/m)	y_S (m)
Measure R04	0.0023	0.0098	56381.3	0.017
Measure R06	0.0023	0.0223	58270.6	0.0166
Measure R20	0.0018	0.0348	57938.2	0.0164
Measure R19	0.0023	0.047	52264.3	0.0167
Measure R16	0.002	0.0523	51051.7	0.016
Measure R26	0.0011	0.0672	39943.9	0.0148

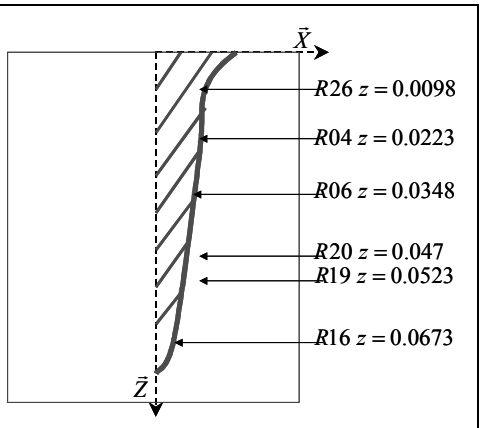

Table 1 : The results of the P_W and y_S estimations

The aim of this part is the identification of the experimental value of P_W and y_S. The electron beam parameter is chosen to $W_{FE} \approx 0.000353$ ($\phi_E = 1\,mm$). The initial set of the parameters is the one used for the theoretical previous numerical applications: $P_W = 5000\,W/m$, $y_S = 0.01\,m$. The inverse problem is solved until the cost function is stabilized or the criterion

$\left\|P^{k+1}-P^{k}\right\|/\left\|P^{k}\right\| \le \varepsilon_3$ is validated ($\varepsilon_3 = 1\%$). The table n°1 gives the results of the P_W and y_S estimations. For the depths $z = \{2.23\,cm; 3.48\,cm; 4.7\,cm; 5.23\,cm\}$. All power P_W and source position y_S values are quite the same: $52000\,W/m\left(z \approx 5\,cm\right) \le P_W \le 58000\,W/m\left(z \ge 4\,cm\right)$ and $y_S \approx 0.0165\,m$. The figure 16 shows an example of the comparison between the experimental and calculated temperatures.

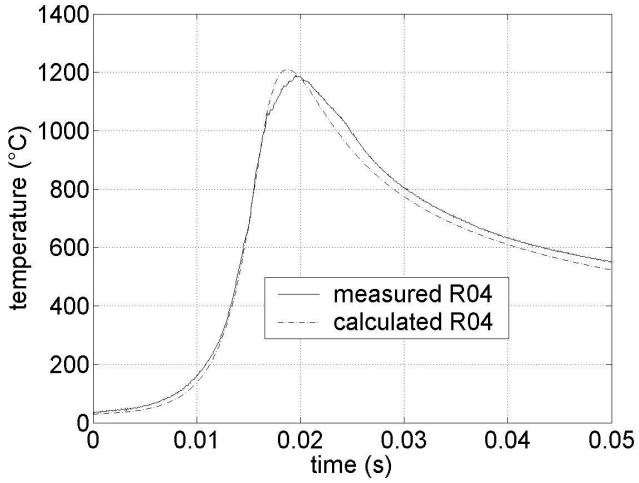

Figure 16 : Comparison between measured and calculated temperatures at $\left(\mathrm{x} = 2,3\ \mathrm{mm}; \mathrm{z} = 22,3\ \mathrm{mm}\right)$

Excepted for the maxima of the temperature, we find a good agreement between the measured and calculated temperatures especially during the heating and cooling phases of the thermal cycles. Consequently in this central zone of the welding, the 2D quasi steady model (x, y) and the Gaussian source modelise quite well the heat transfer. Some problems stay because we take constant thermophysical proprieties.

On the other hand, at the foot (z~67.3mm) and the head of the weld bead (z~9.8mm), we have difficulties to fit the thermal cycle. At the foot of the weld bead, we have a good agreement between measured and calculated kinetics until $y \le 25\,mm$. Beyond we have a cooling temperature measured faster than calculated temperature probably due to the matter below the weld bead which pumps the heat. The bidimensionnal model is not valid. The estimated power P_W seems to be good and is less than the values estimated in the middle of the weld bead. The estimated source position y_S at the foot of the weld bead let thinking that the electron beam is sloped forward. This analysis is unrealistic. As a matter of fact the delay of the source in the central weld bead is probably due to convective movements of the liquid matter which throw again the energy at the back of the electron beam. It is observed at the head of the weld bead where the convective movements are more important. A throwing up of fused matter at the back brings heat to the surface. This heat is dissipated either by heat radiation transfer towards the exterior surroundings or by conduction. That is why the bidimensionnal quasi steady model can't represent correctly the phenomena. It is shown in the figure 17 where we compare measured and calculated kinetics for measurements at the head of the weld bead. Due to the convective energy contribution at the back of the electron beam the experimental kinetic is hotter at cooling. In reality, near to the surface, we should modelise the source with a decentred ellipsoid Gaussian instead of a circular Gaussian. However, we tried few values of electron beam diameter to validate our Gaussian model:

$W_{FE} = \{3.53\ 10^{-4}; 2.32\ 10^{-3}; 4.2\ 10^{-3}\}$ ($\phi_E = \{1\ mm, 7\ mm, 12\ mm\}$ respectively). We show that the cost function decreases when the electron beam diameter increases. At the same time, the source position moves back and the power increases. This result confirms the hypothesis of the rejected energy at the back of the electron beam. Nevertheless this increase of the diameter is limit: in the figure 17 the temperature calculated for $\phi_E = 12\ mm$ rises faster than the measured temperatures. Large diameters produce a premature augmentation of the temperature at the front of the electron beam.

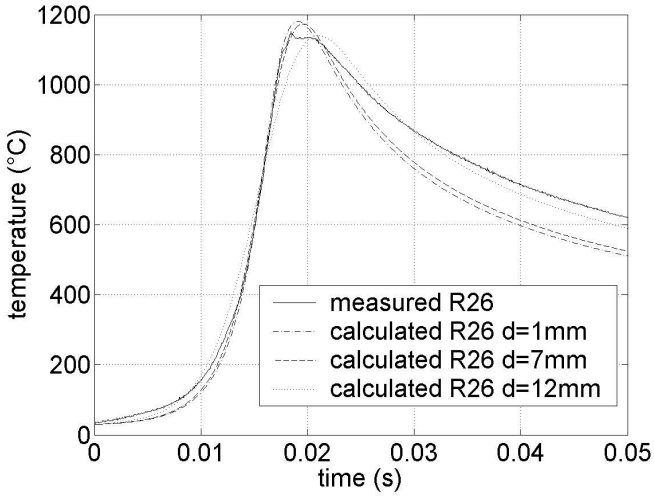

Figure 17 : Comparison between measured and calculated temperature at $(x = 2,3\ mm; z = 9,8\ mm)$

5.2 Estimation of the function with the Iterative Regularisation Method

The significant number of the measurement points as a private individual in the vicinity of surface enables us to make some remarks. First of all, calculation was carried out up to 300 iterations. In a way identical to the theoretical cases [16], it is shown that the decrease is very fast in the first 20 iterations at the time of convergence towards the density of dissipated power. Thereafter, we note a slower variation after a hundred iterations. At this iteration stage, the estimated source evolves very slowly. The forms of source obtained enable us to note that: first, it is impossible to obtain a correct distribution according to the transverse direction (an average value is obtained), second, the distribution according to time follows a law of the Gaussian type (figure 19) except close to the surface (figure 18) where it appears a quantity of considerable energy to the back of the beam certainly related to the fused metal rejection.

Moreover, in figure 20, we can note that the distribution of energy is a depth function with first of all an energy zone near to the surface, then an average value on a middle part of the welding and finally an attenuation of the values to the root of the welding. The figure 21 shows a comparison of the estimated powers with the Levenberg Marquardt and the Iterative Regularization Method. We find a good agreement between the two methods. The second gives us more information on the distribution of the source. With the exit of the preceding estimates, we decided to correct the source term in the transverse direction and to impose a Gaussian form. Indeed, for lack of constraint, the method of iterative regularization leads to a spreading out of energy in this direction which does not make it possible to obtain the correct limits of the fused and heat affected zones compared to the experiment. Figures 22 and 23 present the new forms of source obtained starting from the estimated sources of figures 18 and 19.

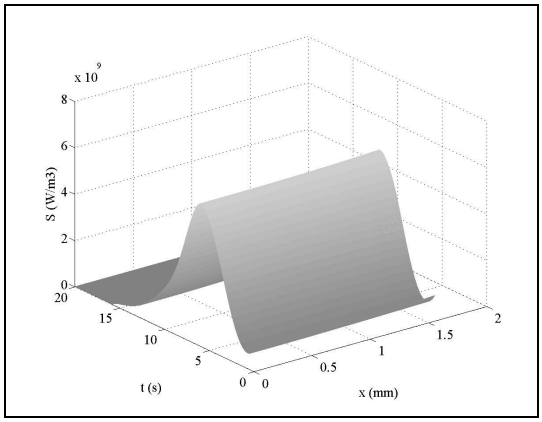

Figure 18. Estimated source at z = 2.47 mm.

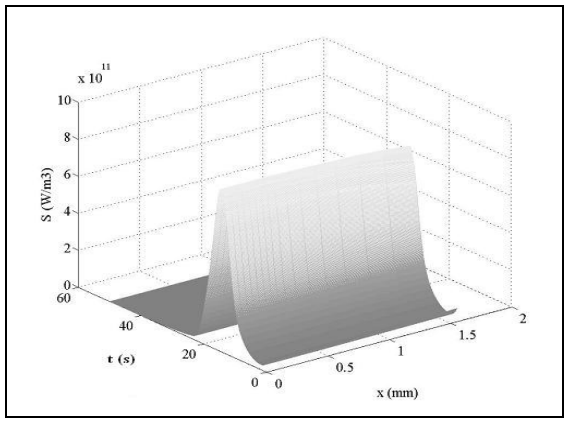

Figure 19. Estimated source at z = 67.37 mm.

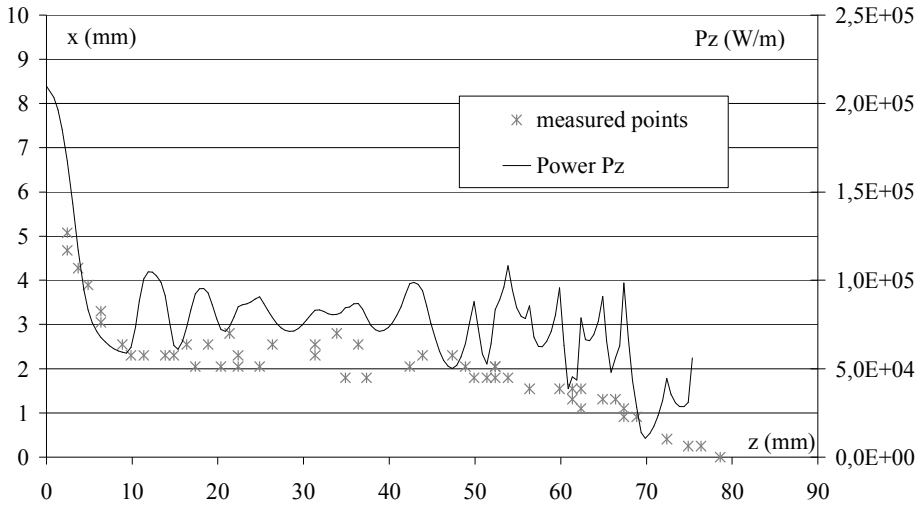

Figure 20. Power density.

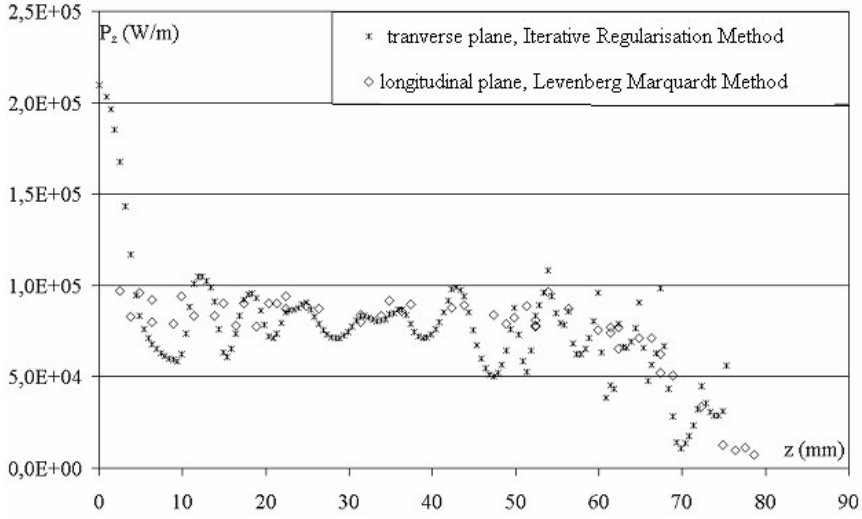

Figure 21: Comparison between the two methods

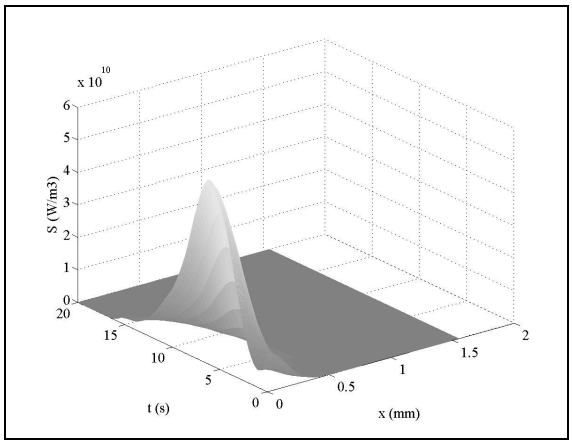

Figure 22. Optimal source at z = 2.47 mm.

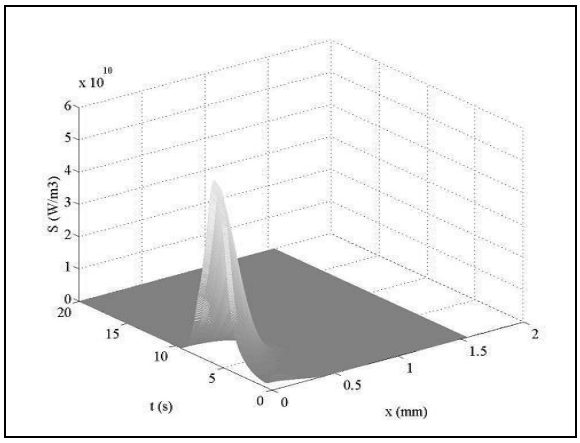

Figure 23. Optimal source at z = 67.37 mm.

6 CONCLUSIONS

The objective of this work was to estimate a source term in the case of the EB welding process. A quasi stationary linear model based on a longitudinal plane 2D and a transient thermometallurgical model based on a transverse plane 2D were carried out. The results show that we have no possibility to correctly describe the energy distribution in the transverse direction e.g. the diameter of the electron beam. An average and constant value is obtained according to this direction. On the other hand, the distributions according to the direction of welding (y or t) and the depth (z) give us relevant indications. Moreover, the analysis of the energy integral according to depth z shows that the energy distribution is uniform for depths $8 < z < 65$ mm and that it varies at the head and foot of the weld. In the foot of the weld, the power density attenuates while at the head of the weld, the matter rejection accentuates this density. Finally, in order to propose a form of optimal source, and in order to circumvent the difficulty related to the transverse distribution of the energy, we proposed to distribute the average energy estimated in the transverse direction in a Gaussian form. A final analysis of the forms of the fused and heat affected zones shows a difficulty in finding the limit of the fused zone. On the other hand, the limit of the heat affected zone is very well found. In the future, we will work on the estimation of a 3D source term.

ACKNOWLEDGEMENT

The authors acknowledge the CESMAN – DCN Indret for the weld joints.

REFERENCES

[1] J.V. Beck, B. Blackwell and C.R. St Clair, Inverse Heat Conduction Ill Posed Problems, Wiley, New York, 1985.

[2] O.M. Alifanov., E.A. Artyukhin and S.V. Rumyantsev, Extreme Methods for Solving Ill-posed Problems with Applications to Inverse Heat Transfer Problems, Begell House, New York, 1995.

[3] Y. Jarny, M.N. Ozisik and J.P. Bardon, A general optimization method using adjoint equation for solving multidimensional inverse heat conduction, Int. J. Heat Mass Transfer 34 (1991) 2911-2919.

[4] A.J. Silva Neto and M.N. Ozisik, Two dimensional inverse heat conduction problem of estimating the time-varying strengh of a line source, J. Appl. Phys. 71 (1992) 5357-5362

[5] C. Le Niliot, The boundary element method for the time varying stengh estimation of point heat sources: application to a two-dimensional diffusion system, Numer. Heat Transfer B 33 (1998) 301-321.

[6] C. Le Niliot and P. Gallet, Infrared thermography applied to the resolution of inverse heat conduction problems : recovery of heat line sources and boundary conditions. Rev. Gen. Therm. 37 (1998) 629-643.

[7] S. Peneau, J.P. Humeau and Y. Jarny, Front motion and convective heat flux determination in a phase change process, Inverse Problems in Eng. 4 (1996) 53-91.

[8] R. Keanini and N. Desai, Inverse finite element reduced mesh method for predicting multidimensional phase change boundaries and nonlinear solid face heat transfer, Int. J. Heat Mass Transfer 39 (1996) 1039-1049.

[9] Y.F. Hsu, B. Rubinsky and K. Mahin, An inverse finite element method for the analysis of stationary arc welding processes, J. Heat Transfer 108 (1986) 734-741

[10] Y. Ruan and N. Zabaras, An inverse finite element technique to determine the change of phase interface location in two dimensional melting problems, Commun. in Appl. Numer. Meth. 7 (1991) 325-338.

[11] N. Zabaras, Adjoint methods for inverse free convection problems with application to solidification processes, Computational Methods for Optimal Design and Control (Birkhauser Series in Progress in Systems and Control Theory), (Eds. J. Borggaard, E. Cliff, S. Schreck and J. Burns), Birkhauser, pp. 391-426, 1998 (Proceedings of the U.S. Air Force Optimum Design and Control Symposium, held at Arlington, VA, September 30 -- October 3, 1997).

[12] V. A. Karkhin, V.V. Plochikhine and H.W. Bergmann, Solution of inverse heat conduction problem for determining heat input, weld shape, and grain structure during laser welding, Science and Technology of Welding and Joining 7 **(4)** (2002) 224-231.

[13] D.D.Doan, F. Gabriel, Y. Jarny, P. Le Masson, Simulation of a weld pool interface motion by a variational inequality approach ; Fluid structure interaction and moving boundary problems, Edt WIT press, (2005) 671-681.

[14] M.N. Osizik, H.R.B. Orlande, Inverse heat transfer: fundamentals and applications, Taylor and Francis, New York,(2000).

[15] M. Costantini, Simulation numérique du soudage par faisceau d'électrons - contribution au développement d'un modèle prédictif de l'apport d'énergie, Thèse de l'université Paris 6 (1995).

[16] J. Guo, Estimation de la distribution énergétique induite par un faisceau d'électrons dans un matériau métallique – Application au cas du soudage d'un acier. Thèse de l'université de Bretagne Sud (2005).

[17] P. Rogeon, D. Couedel, D. Carron, P. Le Masson and J.J. Quemener, Numerical simulation of electron beam welding of metals : sensitivity study of a predictive model, Mathematical Modelling of Weld Phenomena 5, (Eds. H.Cerjak and H.K.D.H. Bhadeshia), Institute of Materials (2001) 913-943.

[18] D. Couedel , P. Rogeon, P. Le Masson, M. Carin, J.C. Parpillon, R. Berthet, 2D-Heat transfer modelling within limited regions using moving sources : application to electron beam welding, Int. Journal of Heat and Mass Transfer, vol. 46, pages 4553-4559, (2003)

[19] Manuel d'utilisation "sysweld", Systus International (1994).

[20] J. Leblond and J. Devaux, A new kinetic model for anisothermal metallurgical transformations in steels including effect of austenite grain size ; Acta Metallurgica, 32 **(1)** (1984) 137-146.

[21] D.P. Koistinen and R.E. Marburger, A general equation prescribing the extent of austenite-martensite transformation in pure iron-carbon alloys and plain carbon steels; Acta. Metallurgica, 7 (1959) 59.

[22] M. Carin, P. Rogeon, D. Carron, P. Le Masson and D. Couedel, Numerical simulation of electrons beam welding and instrumental technique, Revue Européenne des Eléments Finis, 13 **(3-4)** (2004) 247-267.

[23] Y. Arata, Evaluation of beam characteristics by the ab test method, Plasma, electron and laser beam technology, Metals Park, Ohio/USA : American Society for Metals, (1986) 177-189.